

Original article

Europium-activated phosphors for use in X-ray detectors of medical imaging systemsI. Kandarakis¹, D. Cavouras^{1*}, G. S. Panayiotakis², D. Triantis³, C. D. Nomicos³¹ Department of Medical Instrumentation Technology, Technological Educational Institution of Athens, Ag. Spyridonos Street, Aigaleo, GR-12210 Athens, Greece² Department of Medical Physics, Medical School, University of Patras, GR-265 00 Patras, Greece³ Department of Electronics, Technological Educational Institution of Athens, Ag. Spyridonos Street, Aigaleo, GR-12210 Athens, Greece

Received 17 March 1997; Revision received 25 July 1997; Accepted 21 August 1997

Abstract. Three europium-activated phosphors $Y_2O_2S:Eu$, $Y_2O_3:Eu$, and $YVO_4:Eu$ emitting red light were studied to investigate their suitability for radiographic cassettes or digital imaging systems. Screens were prepared from phosphor powders with various coating thicknesses by sedimentation. To assess phosphor light producing efficiency in relation to patient dose, each screen was X-rayed using 40–120 kVp and the number of light photons emitted per X-ray incident was experimentally and theoretically evaluated. Additionally, the capability of the emitted light to sensitize films or to generate electrons in silicon photodiodes used in digital imaging systems was examined. $Y_2O_2S:Eu$ screens were most efficient in light emission, and when combined with either red sensitive films or Si photodiodes, they were found superior to $Y_2O_3:Eu$ or $YVO_4:Eu$ screens in film grain or electron signal generation. In many cases they were also found superior to terbium-activated phosphors. Provided that several problems related to industrial production (special dyes, reflective backing, crossover effects) are dealt with, those europium-activated screens could be employed in low-tube-voltage radiographic applications.

Key words: X-ray screens – X-ray luminescence – Spectral matching

Introduction

In most X-ray imaging modalities X-rays are converted into light that darkens a radiographic film or generates photoelectrons either in the photocathode of a fluoroscopic image intensifier or in the silicon (Si) photodiode of a digital imaging system. Terbium-activated phosphors

$Gd_2O_2S:Tb$, $La_2O_2S:Tb$ and $Y_2O_2S:Tb$ have been considered to be the most efficient X-ray-to-light converters [1–4] employed in radiography. However, in digital imaging systems the emitted light is not efficiently detected by the Si photodiodes, because the latter are not adequately sensitive at these wavelengths (500–550 nm); only 45–55 % of the light produced by $Gd_2O_2S:Tb$ or $Y_2O_2S:Tb$ is registered by the Si photodiode [3]. On the other hand, europium-activated phosphors emit at wavelengths towards the red region of the light spectrum which is closer to the maximum sensitivity of the Si photodiode. These red emitting phosphors should exhibit adequate matching with some films exhibiting high sensitivity to red light such as those used in laser imagers.

In this study three europium-activated yttrium based phosphors, $Y_2O_2S:Eu$, $Y_2O_3:Eu$ and $YVO_4:Eu$, were examined for use in radiographic cassettes and in detectors of digital X-ray imaging systems. The detector of a digital system is considered to consist of a phosphor screen connected to photodiode arrays via fiber optics [3].

The combined efficiency of each phosphor material coupled either to a film or a photodiode array was evaluated considering the following parameters:

1. The intensity of the light emitted per incident X-ray or light emission efficiency
2. The spectrum of the light and its compatibility to red sensitive films and to Si photodiodes
3. The light detector conversion efficiency, which describes the capability of the light detector (film or photodiode) to convert light photons into useful signal, i.e. developed silver halide film grains or electrons in the photodiode output

Results were compared with data obtained under similar conditions on terbium activated phosphors.

Correspondence to: D. Cavouras

*Present address: Department of Medical Instrumentation Technology, 37–39 Esperidon Street, Kallithea 17671, Athens, Greece

Materials and methods

Phosphors were supplied in powder form by Lumilux. From each phosphor material seven screens of thicknesses ranging from 20 to 160 mg/cm² were prepared by sedimentation. Screens were irradiated by a Siemens Stabilipan machine with X-ray tube voltages ranging from 40 to 120 kVp with screens positioned at 70 cm from the focal spot of the X-ray tube. The fluorescent light flux emitted during irradiation was recorded by an EMI 9558 QB photomultiplier connected to a Cary 401 electrometer. The emitted light flux was measured at both sides of the screen, the irradiated front side and the non-irradiated rear side, in order to simulate light emission from both screens included in a radiographic cassette [2]. For determining the phosphor's light emission efficiency, X-ray exposure measurements were performed employing an appropriate for the X-ray energies used (40–120 kVp) PTW dosimeter (ionization chamber type no. 23333, test certificate no 890802, PTW, Freiburg, Germany) positioned at 70 cm from the tube's focal spot and being in this work. The X-ray exposure rate was converted to energy fluence rate using an appropriate conversion factor [5]. Details of the experimental setup are given elsewhere [2, 4, 6].

The light emission efficiency N_ϕ may be defined as the number of light photons emitted by the phosphor screen per X-ray incident and is expressed by (see Appendix):

$$N_\phi = \frac{\Psi_L}{\Psi_X} \frac{E}{hc} \frac{1}{\lambda} \quad (1)$$

where Ψ_L is the light photon energy flux, Ψ_X is the X-ray photon energy flux, E is the energy of the incident X-ray photon, h is Planck's constant, c is the light velocity, and λ is the mean wavelength of the emitted light photons. Ψ_L was measured by means of the photomultiplier, Ψ_X was determined by measuring the X-ray exposure rate by the dosimeter and converting it into energy flux [2, 5]. λ was determined by measuring the light emission spectrum using an Oriel 7240 grating monochromator. N_ϕ was determined at tube voltages between 40 and 120 kVp, mostly employed in radiography.

The light emission efficiency N_ϕ was also mathematically modeled (see Appendix) as a function of light scattering (s), light absorption (a) and intrinsic X-ray-to-light conversion efficiency (η_C); the latter gives the percentage of absorbed X-ray energy that is converted into light within the phosphor material. Values for parameters a , s and η_C were determined by fitting the experimental data with the mathematical model employing the Levenberg-Marquard method [7]. Thus, all coefficients related to light generation and light propagation phenomena inside the screen material were estimated.

Light spectra emitted by each phosphor material were measured by the Oriel monochromator and were compared with the spectral sensitivity of the Si photodiode and with the sensitivity of two well-known photographic emulsions (Agfa Scopix LT 2B film and Fuji

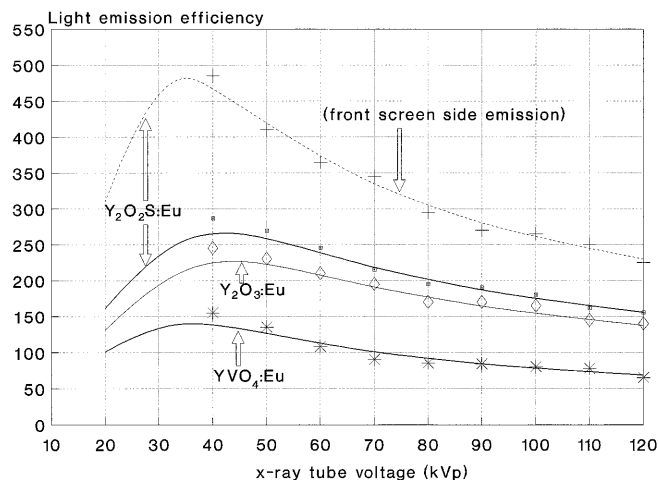


Fig. 1. Variation of the light emission efficiency (light photons emitted per incident X-ray) with X-ray tube voltage (kVp) for $Y_2O_2S:Eu$, $Y_2O_3:Eu$ and $YVO_4:Eu$ of 80 mg/cm². *Solid lines* correspond to curves fitted through experimental data from the non-irradiated rear side of the screen. *Dotted line* corresponds to light emission from the irradiated front side of screen of $Y_2O_2S:Eu$. *Points* represent experimental data. *Curves below 40 kVp* correspond to calculated data

LI-HM). Thus, the suitability of the three phosphors to be combined with those light detectors was investigated. Precise spectral compatibility was accurately calculated by determining the spectral matching factor (see Appendix) [8, 9]. The values of the spectral matching factor range between 0 and 1 providing a quantitative description of how well the phosphor's light spectrum matches the sensitivity of films, photodiodes or other light detectors. Matching factor 1 indicates perfect light detection and 0 signifies that no light is detected.

The net effect of using a phosphor in combination with a specific light detector, such as a film or a photodiode, can be described by the combined efficiency (N_{cmb}). The latter may be defined as the product of (a) the number of light photons (N_ϕ) emitted per X-ray incident on the phosphor, (b) the spectral matching factor (a_s) of the combination and (c) the light detector conversion efficiency (η_{LC}):

$$N_{cmb} = N_\phi a_s \eta_{LC} \quad (2)$$

η_{LC} gives the number of developed silver halide grains on the radiographic film or the number of electrons produced in the Si photodiode per absorbed light photon. In the case of digital systems η_{LC} is given by the product of the light collection efficiency of the intervening optical fiber and the quantum conversion efficiency of the photodiodes. Values for η_{LC} were obtained from the literature [1, 3, 10]. N_{cmb} was determined for all the screens as a function of X-ray tube voltage.

Results and discussion

Figure 1 shows the variation of light emission efficiency with X-ray tube voltage for the $Y_2O_2S:Eu$, $Y_2O_3:Eu$ and

Table 1. Light generation (η_c) and light propagation (a,s) properties of phosphors

Phosphors	Intrinsic efficiency (η_c)	Optical scattering (s)	Optical absorption (a)
$Y_2O_2S:Eu$	0.110	249.76	0.45
$Y_2O_3:Eu$	0.095	416.29	0.75
$YVO_4:Eu$	0.070	582.81	1.05
$Y_2O_2S:Tb$	0.180	499.55	0.90
$Gd_2O_2S:Tb$	0.200	499.55	0.90

Table 2. Spectral matching factors

Phosphors	Optical detectors				
	Si photodiode	Agfa LT 2B	Fuji LH	Agfa Curix Ortho GS	Fuji UM-MH
$Y_2O_2S:Eu$	0.653	0.861	0.777	–	–
$Y_2O_3:Eu$	0.663	0.924	0.848	–	–
$YVO_4:Eu$	0.664	0.957	0.872	–	–
$Gd_2O_2S:Tb$	0.543	–	–	0.692	0.698
$Y_2O_2S:Tb$	0.411	–	–	0.827	0.802

–: non desirable combination

and $YVO_4:Eu$ 80 mg/cm² screens. For each phosphor screen rear-side light emission measurements are presented. Additionally, front-side measurements for the $Y_2O_2S:Eu$ screen are shown. Curves concern best fittings through the experimental measurements, using formulas (B1) of the Appendix in the Levenberg-Marquard method. Light emission efficiency decreases slowly with tube voltage after approximately 40 kVp due to a corresponding decrease in the phosphor's efficiency to absorb X-rays (η_0) with increasing X-ray energy. The $Y_2O_2S:Eu$ screen was found to be the most efficient of the three in the whole range of X-ray tube voltages, whereas the performance of the $Y_2O_3:Eu$ screen was intermediate. Similar performance of the three phosphors was also observed for screens at different coating thicknesses. This is due to the fact that among the three phosphors $Y_2O_2S:Eu$ screens display the highest intrinsic X-ray-to-light conversion efficiency (η_c) and the lower light attenuation coefficients (a, s) followed by those of $Y_2O_3:Eu$ (Table 1). Light emission from the irradiated front side of the $Y_2O_2S:Eu$ screen was found higher than the corresponding emission from the non-irradiated rear side. This is expected since X-rays are mainly absorbed at depths close to the surface of the irradiated side. Thus, light photons generated within the phosphor material are easier transmitted towards the irradiated surface.

In Fig. 2 the measured light emission spectra of the three phosphors are presented together with the spectral sensitivity distributions of the Si photodiode and of two red sensitive films. Values for spectral matching factors corresponding to various combinations of the three phosphors with the light detectors are given in Table 2. The best combination was that of the $YVO_4:Eu$ phosphor with the Agfa Scopix LT 2B film. The compatibility of $Y_2O_3:Eu$ or $YVO_4:Eu$ with the Si photodiode was better than that of $Y_2O_2S:Eu$ and well above the compatibility of the terbium-activated phos-

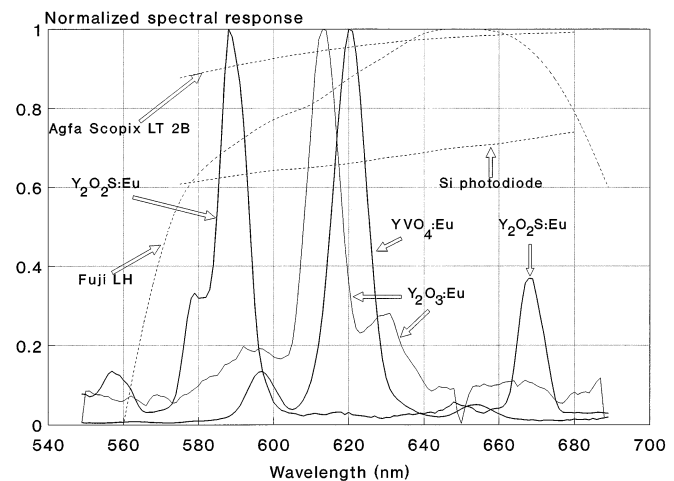


Fig. 2. Measured spectra of light emitted by the three phosphors with spectral sensitivities of the Agfa Scopix LT 2B film, Fuji LH film and Si photodiode

phor $Gd_2O_2S:Tb$. $Y_2O_2S:Eu$ shows lower values of matching factors with the red sensitive light detectors due to its spectral components at lower wavelengths towards the yellow region of the optical spectrum (Fig. 2). In the same table the matching factor of the $Gd_2O_2S:Tb$, which is the phosphor mostly employed in radiography, with some green sensitive radiographic films and the Si photodiode, are also given for comparison. In most cases the matching factors of the red emitting europium-activated phosphors were higher than those of $Y_2O_2S:Tb$ and $Gd_2O_2S:Tb$ usually employed in radiography. This suggests that europium-activated phosphors give better combinations with light-sensitive detectors used in digital and conventional radiography.

$Y_2O_2S:Eu$ screens coupled to red sensitive films or to photodiode arrays gave best combined efficiency

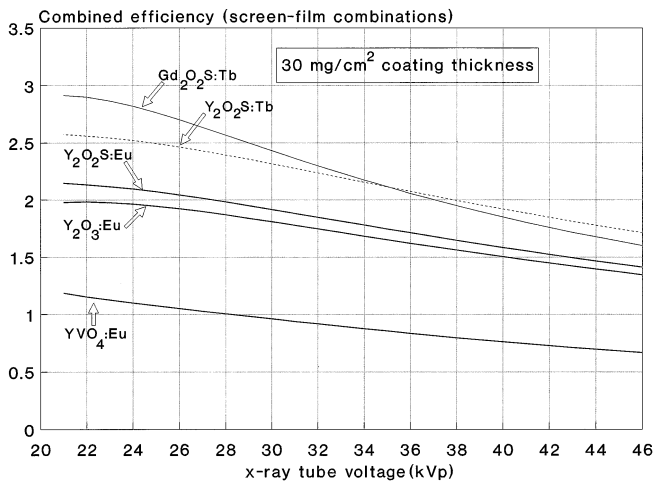


Fig. 3. Variation of the number of developed silver halide grains (combined efficiency) per incident X-ray with tube voltage for Y₂O₂S:Eu, Y₂O₃:Eu and YVO₄:Eu screens in combination with Agfa Scopix LT 2B film and for Gd₂O₂S:Tb and Y₂O₂S:Tb screens in combination with Agfa Curix Ortho GS film. All screens had coating thickness of 30 mg/cm². Curves below 40 kVp correspond to calculated data

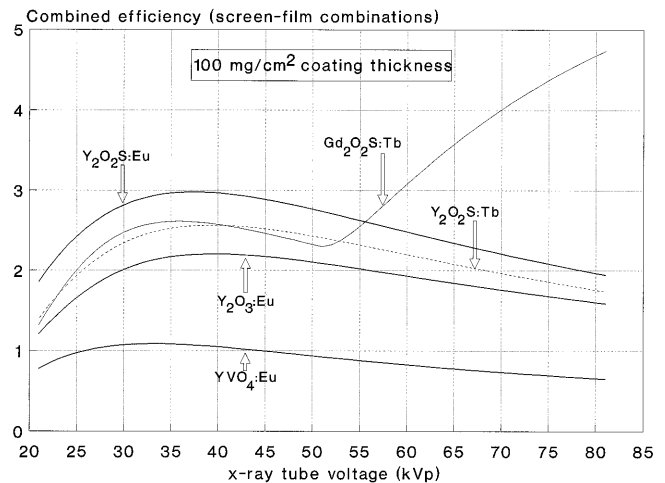


Fig. 5. Variation of the number of developed silver halide grains (combined efficiency) per incident X-ray with tube voltage for Y₂O₂S:Eu, Y₂O₃:Eu and YVO₄:Eu screens in combination with Agfa Scopix LT 2B film and for Gd₂O₂S:Tb and Y₂O₂S:Tb screens in combination with Agfa Curix Ortho GS film. All screens had coating thickness of 100 mg/cm². Curves below 40 kVp correspond to calculated data

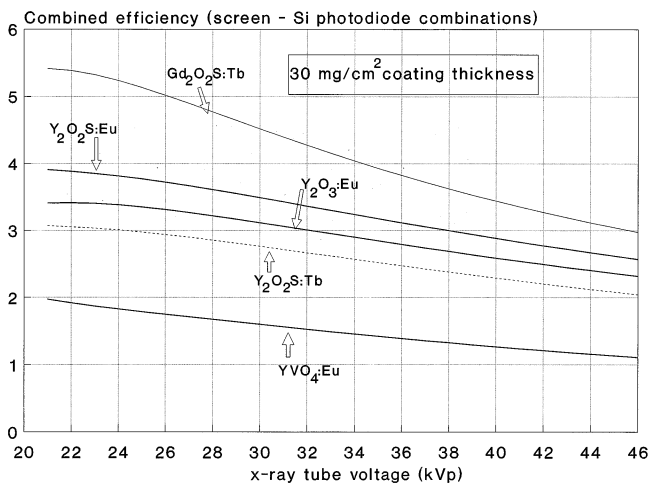


Fig. 4. Variation of the number of electrons in digital detector output (combined efficiency) per incident X-ray with tube voltage for Y₂O₂S:Eu, Y₂O₃:Eu, YVO₄:Eu, Gd₂O₂S:Tb and Y₂O₂S:Tb screens in combination with the Si photodiode. All screens had coating thickness of 30 mg/cm². Curves below 40 kVp correspond to calculated data



Fig. 6. Variation of the number of electrons in digital detector output (combined efficiency) per incident X-ray with tube voltage for Y₂O₂S:Eu, Y₂O₃:Eu, YVO₄:Eu, Gd₂O₂S:Tb and Y₂O₂S:Tb screens in combination with the Si photodiode. All screens had coating thickness of 100 mg/cm². Curves below 40 kVp correspond to calculated data

(N_{cmb}) results as compared with the other two phosphors (Figs. 3–6). These figures present results obtained for the 30- and 100-mg/cm² screens of Y₂O₂S:Eu, Y₂O₃:Eu and YVO₄:Eu considering light emission from the non-irradiated rear side of the screen. Thicknesses of 30 and 100 mg/cm² were selected to simulate mammographic and general X-ray imaging conditions, respectively. Results on Gd₂O₂S:Tb and Y₂O₂S:Tb laboratory-prepared phosphor screens in combination with green sensitive films (Agfa Curix Ortho GS, Fuji UM-MH) or with the Si photodiode are also presented for comparison. In the case of films,

an average value of 0.01 was employed for the light detector conversion efficiency (η_{LC}) [1], meaning that one developed film silver halide grain corresponds to 100 light photons. For the fiber optics-photodiode system $\eta_{\text{LC}} = 0.04$. At 30 mg/cm², the Y₂O₂S:Eu screen combined with either a red sensitive film or the Si photodiode was found less efficient than the Gd₂O₂S:Tb screen combined either with a green sensitive film or with the Si photodiode (Figs. 3, 4). On the other hand, when the 100-mg/cm² Y₂O₂S:Eu screen was combined either with a film or with the Si photodiode, it was more efficient than the corresponding

Gd₂O₂S:Tb combinations, for tube voltages lower than 56 kVp (Figs. 5, 6). Additionally, the 100-mg/cm² Y₂O₂S:Eu screen performed better than the corresponding Y₂O₂S:Tb screen for all combinations and tube voltages. Finally, Y₂O₃:Eu was better than Y₂O₂S:Tb when both phosphors were coupled to the Si photodiode and for both 30- and 100-mg/cm² coating thicknesses. Yttrium-based europium-activated phosphors are adequately efficient in combination with red sensitive films and Si photodiodes, because although they have lower intrinsic conversion efficiencies, they exhibit low light attenuation and very good to excellent spectral compatibility with light detectors. Thus, they could be used in both digital and conventional radiographic applications especially at low tube voltages as in radiography of the hands, feet, vessels, etc. However, since this work involves laboratory-prepared test screens, it will be a long time before they are manufactured for radiographic applications. Problems such as addition of special dyes or reflective backing, and image blurring due to crossover effects, will have to be addressed.

Appendix

Appendix A: Experimental light emission efficiency

The light emission efficiency is defined as follows:

$$N_{\Phi} = \frac{N_L}{N_X} \quad (A1)$$

where N_L is the number of emitted light photons generated by N_X incident X-ray photons. N_L and N_X are obtained from the measured X-ray energy flux Ψ_X and the light energy flux Ψ_L as follows:

$$\Psi_X = \frac{N_X E}{\Delta a \Delta t} \quad (A2)$$

$$\Psi_L = \frac{N_L E_L}{\Delta a \Delta t} \quad (A3)$$

where E is the energy of an incident X-ray photon, E_L is the energy of an emitted light photon given by hc/λ , and Δa and Δt are units of area and time. From Eqs. A(1)–A(3):

$$N_{\Phi} = \frac{\Psi_L}{\Psi_X} \times \frac{E_X \lambda}{hc} \quad (A4)$$

For polyenergetic X-ray beams, N_{Φ} is averaged over the whole X-ray spectrum

$$N_{\Phi} = \frac{\int_0^{E_{\max}} N_{\Phi}(E) S_X(E) dE}{\int_0^{E_{\max}} S_X(E) dE} \quad (A5)$$

where S_X is the X-ray spectrum [11] and $N_{\Phi}(E)$ is the light emission efficiency for monoenergetic X-rays.

Appendix B: Theoretical light emission efficiency

Light emission efficiency was theoretically evaluated considering that it is the product of the following quantities [12, 13]:

$$N_{\Phi} = \eta_Q \eta_C G_L(a, s) E/E_L \quad (B1)$$

where η_Q is the X-ray quantum detection efficiency (QDE), expressing the fraction of incident X-ray quanta detected by the screen, which is approximately given by:

$$\eta_Q = 1 - \exp[-\mu T] \quad (B2)$$

where μ is the mass attenuation coefficient of the phosphor for X-rays calculated using published data [14, 15], and T is the screen coating thickness; η_C is the intrinsic X-ray to light conversion efficiency, giving the fraction of absorbed X-ray energy converted to light within the phosphor material; $G_L(a, s)$ is the light transmission efficiency, expressing the fraction of light produced that reaches the screen output [12], a and s being the coefficients of light absorption and light scattering; E and E_L are defined in Eqs. (A2) and (A3).

Appendix C: Spectral matching factor

The spectral matching factor was calculated by the formula [6, 9]

$$a_S = \frac{\int_{\lambda_1}^{\lambda_2} S_P(\lambda) S_D(\lambda) d\lambda}{\int_{\lambda_1}^{\lambda_2} S_D(\lambda) d\lambda} \quad (C1)$$

where λ_1 and λ_2 are the lower and upper wavelength limits of the spectrum, $S_P(\lambda)$ is the normalized spectrum of the phosphor screen, experimentally determined with an Oriel 7240 grating monochromator, $S_D(\lambda)$ is the normalized spectral sensitivity distribution of the optical detector, obtained from manufacturer's data (RS Opto-Devices, data sheet 2135, 1981).

Acknowledgement. This study is dedicated to the memory of G.E. Giakoumakis, leading member of our team, whose work on phosphor materials has inspired us to continue.

References

1. Arnold BA (1979) Physical characteristics of screen-film combinations. In: Haus AG (ed) The physics of medical imaging: recording system, measurements and techniques. American Association of Physicists in Medicine, New York, pp 30–71
2. Giakoumakis GE, Nomicos CD, Yiakoumakis EN, Evangelou EK (1990) Absolute efficiency of rare earth oxysulfide screens in reflection mode observation. *Phys Med Biol* 35: 1017
3. Gurwich AM (1995) Luminescent screens for mammography. *Radiat Mes* 24: 325
4. Kandarakis I, Cavouras D, Panayiotakis G, Agelis T, Nomicos C, Giakoumakis G (1996) X-ray induced luminescence and spatial resolution of La₂O₂S:Tb phosphor screens. *Phys Med Biol* 41: 297
5. Hendee WR (1970) Medical radiation physics. Year Book Medical Publishers, Chicago

6. Cavouras D, Kandarakis I, Panayiotakis G, Evangelou EK, Nomicos CD (1996) An evaluation of the $Y_2O_3:Eu^{3+}$ scintillator for application in medical X-ray detectors and image receptors. *Med Phys* 23: 1965
7. Press WH, Flannery BP, Teukolsky SA, Vetterling WT (1989) Numerical recipes in Pascal: the art of scientific computing. Cambridge University Press, Cambridge
8. Giakoumakis GE (1991) Matching factors for various light-source-photodetector combinations. *Appl Phys A52*: 7
9. Panayiotakis G, Cavouras D, Kandarakis I, Nomicos C (1996) A study of X-ray luminescence and spectral compatibility of europium-activated yttrium-vanadate ($YVO_4:Eu$) screens for medical imaging applications. *Appl Phys* 62: 483
10. Karellas A, Harris LJ, Liu H, Davis MA, D'Orsi CJ (1992) Charged-couple device detector: performance considerations and potential for small-field mammographic imaging applications. *Med Phys* 19: 1015
11. Storm E (1972) Calculated bremsstrahlung spectra from thick tungsten targets. *Phys Rev A5*: 2328
12. Ludwig GW (1971) X-ray efficiency of powder phosphors. *J Electrochem Soc* 118: 1152
13. Hamaker H (1947) Radiation and heat conduction in light-scattering material. *Philips Res Rep* 2: 55
14. Saloman EB, Hubbell JH, Scofield JH (1988) X-ray attenuation cross sections for energies 100 eV to 100 keV and elements $Z = 1$ to $Z = 92$. *At Data Nucl Data Tables* 38: 1
15. Storm E, Israel H (1967) Photon cross sections from 0.001 to 100 MeV for elements 1 through 100. Report LA-3753. Los Alamos Scientific Laboratory, University of California

Book review

European
Radiology

Revel, D. and others: Imagerie Artérielle Non-Invasive: Modalités Techniques et Analyse Critique. Paris: Editions Masson 1996. 240 pp., (ISBN 2-225-85349-5), BF 3300.00.

It was a pleasure to review this book in which Dr. Revel has brought together the experience of well known experts in the different fields of noninvasive vascular imaging.

The book consists of five chapters. In the first chapter, the different modalities for noninvasive imaging of the thoracic aorta are discussed: transthoracic and transesophageal sonography, spiral CT angiography (CTA) and magnetic resonance angiography (MRA). This part is illustrated by state-of-the art images obtained with the different modalities, e.g. colored surface-rendered displays calculated from data obtained with CTA.

The second chapter consists of a description of the various abnormalities of the supra-aortic vessels and their presentation on Doppler ultrasound (US), spiral CTA and MRA. The following features are discussed with regard to US of the carotid arteries: normal findings, morphologic aspects of carotid plaques, and findings in cases of stenosis, thrombosis and dissection. Also discussed are lesions of the vertebral arteries and subclavian arteries. In the second and third part of this chapter, an extensive overview is given of the technique, indications and limitations of CTA and MRA of the carotid arteries.

The third chapter focuses on the investigation of the renal arteries by Doppler US, CTA and MRA. The different Doppler criteria proposed by different authors to evaluate renal artery stenoses are well summarized, as well as the optimal CT technique and the two classic MR techniques (time-of-flight and phase contrast MRA).

Chapter 4 covers the abdominal aorta and its branches, with particular emphasis on the evaluation of abdominal aortic aneu-

rysms. At the end of this chapter, an interesting discussion focuses on two promising developments: spiral CT and 'first pass' contrast-enhanced MRA.

The fifth and last chapter discusses some novel concepts in vascular imaging: endovascular US, a new system for computerized three-dimensional angiography ('le morphomètre') and, finally, a description of current concepts and potential future developments in stenosis quantification.

This book is unique because it offers state-of-the-art information on new imaging modalities in a rapidly evolving area of diagnostic radiology. All chapters are well written and the illustrations are of high quality. The references are up to date (as far as possible). A particularly interesting feature of the book is that it offers much more than just a description of imaging findings: in each chapter and for each technique, much emphasis is put on technical aspects ('how to do it'), potential pitfalls, anatomic variants, limitations, and comparison of modalities used for image display. The diagnostic accuracy of the different techniques as reported in previously published papers is well summarized and, at the end of each chapter, a short summary comparing the different techniques is provided. My only criticism would be that contrast-enhanced MRA and the potential role of new MR blood pool contrast agents deserve more attention. MRA of the renal arteries, for instance, is nowadays performed using fast injection of contrast medium in combination with breath-hold three-dimensional scanning.

In conclusion, the authors have done an admirable job. Taking into account the low price of this book and the enormous amount of information it provides, I can recommend it to anyone eager to learn more about noninvasive vascular imaging.

L. Van Hoe, Leuven